Mixed Cu^+ and Zn^{2+} Coordination in the DNA-Binding Domain of the AMT1 Transcription Factor from *Candida glabrata*†

Joanne L. Thorvaldsen,‡ Andrew K. Sewell,‡ Amie M. Tanner,‡ John M. Peltier,§ Ingrid J. Pickering,∥ Graham N. George,∥ and Dennis R. Winge*,‡

Departments of Medicine, Biochemistry, and Medicinal Chemistry, University of Utah Health Science Center, Salt Lake City, Utah 84132, and Stanford Synchrotron Radiation Laboratory, Stanford University, SLAC P.O. Box 4393, Stanford, California 94309

Received April 11, 1994; Revised Manuscript Received June 13, 1994®

ABSTRACT: AMT1 is the transcription factor required for Cu-induced expression of metallothionein genes in the yeast *Candida glabrata*. The copper-binding, DNA-binding domain of AMT1 has been purified after expression of an AMT1 synthetic gene in bacteria and was confirmed as active in a gel shift assay. The Cu-activated AMT1 was shown to contain a Cu^+–thiolate tetracopper center and a single Zn^{2+} site. AMT1 is purified as a Cu–Zn protein from bacterial cultures grown in the presence of $CuSO_4$. Chemical analysis suggested that 4.2 ± 0.2 and 1.2 ± 0.2 molar equiv copper and zinc ions bound, respectively. Electrospray mass spectrometry was used to verify that a uniform species was present with 4 Cu^+ ions and 1 Zn^{2+} ion bound per AMT1 molecule. Cu^+ binding to form a tetracopper center occurs cooperatively as shown by electrospray MS of apoAMT1 samples reconstituted with increasing equivalency of Cu^+. Copper–thiolate coordination was indicated by Cu–S charge-transfer transitions in the ultraviolet, luminescence typical of Cu–thiolate clusters and EXAFS. Analysis of the EXAFS of CuZnAMT1 revealed predominantly trigonal Cu^+ coordination and the presence of a polycopper cluster by virtue of a short Cu–Cu distance of 2.7 Å. Zn K-edge EXAFS of Cu_4Zn_1AMT1 and electronic spectroscopy of AMT1 with Co^{2+} substituted for the single Zn^{2+} ion are consistent with tetrahedral Zn^{2+} coordination with thiolate ligands. The Cu-activated AMT1 exhibited a conformation distinct from that of metal-free AMT1 as shown by circular dichroism. DNA binding by AMT1 was dependent on the tetracopper center but was independent of occupancy of the Zn^{2+} site. This is the first report of a single, uniform tetracopper center in a metal-activated transcription factor.

All organisms possess mechanisms to prevent metal ion induced toxicity. The yeasts *Saccharomyces cerevisiae* and *Candida glabrata* respond to copper stress by inducing expression of metallothionein (MT) genes (Hamer, 1986; Thiele, 1992). The induced MT proteins buffer the intracellular copper concentration. The coupling of the copper concentration to MT gene expression is achieved by a Cu^+-responsive transcription factor, designated ACE1 (CUP2) in *S. cerevisiae* (Thiele, 1988; Furst et al., 1988; Welch et al., 1989) and AMT1 in *C. glabrata* (Zhou & Thiele, 1991). ACE1 mediates the Cu-induced expression of the *CUP1* MT gene locus in *S. cerevisiae* (Thiele, 1988; Furst et al., 1988; Welch et al., 1989). AMT1 mediates the Cu-induced expression of three distinct MT genes in *C. glabrata* (Zhou et al., 1992; Thorvaldsen et al., 1993).

ACE1 and AMT1 exhibit a 50% sequence identity in the N-terminal half of each molecule (Furst et al., 1988; Szczypka & Thiele, 1989; Zhou & Thiele, 1991). The homologous N-terminal region is the segment of ACE1 responsible for copper binding and specific DNA binding (Furst et al., 1988). DNA binding by ACE1 is dependent on bound Cu^+ (Furst et al., 1988; Buchman et al., 1989). AMT1 can functionally replace ACE1 in *S. cerevisiae* with retention of Cu-induced expression of the *S. cerevisiae* MT gene, but ACE1 is only minimally effective in mediating Cu-induced expression from *C. glabrata* MT promoters (Thorvaldsen et al., 1993).

We are interested in the mechanism by which copper ions activate ACE1 and AMT1 resulting in induced transcription of MT genes. Our initial studies were of the bacterially expressed DNA-binding domain of ACE1 in which we demonstrated that ACE1 binds 4–6 Cu^+ ions *in vitro* within at least one polycopper cluster (Dameron et al., 1991; Nakagawa et al., 1991). Cysteinyl thiolates appear to be ligands for the polycopper cluster(s) (Dameron et al., 1991; Hu et al., 1990). Detailed EXAFS analysis of CuACE1 suggested that the Cu^+ ions are predominantly trigonally coordinated (Pickering et al., 1993). Eleven of the 12 cysteines in the DNA-binding domain of ACE1 were shown to be critical for transcriptional activation (Hu et al., 1990). The essential 11 cysteinyl residues are conserved in the AMT1 molecule (Zhou & Thiele, 1991).

A number of significant questions regarding the role of Cu^+ in the structure and function of ACE1 and AMT1 remain unresolved. First, no structural studies have been reported on AMT1. Second, the mentioned studies on ACE1 do not establish definitively whether a single polycopper cluster or multiple polycopper clusters exist in the active ACE1. Third,

† This work was supported by the National Institute of Environmental Health Sciences, National Institutes of Health (ES 03817 to D.R.W.). The authors acknowledge support from the National Institutes of Health [5P30-CA 42014] to the Biotechnology Core Facility for protein sequencing and DNA synthesis. Support is also acknowledged from the Utah Regional Cancer Center, Grant 5P30 CA42401, for support of the electrospray mass spectrometry core facility. The SSRL is operated by the Department of Energy, Office of Basic Energy Sciences. The SSRL Biotechnology Program is supported by the National Institutes of Health, Biomedical Resource Technology Program, Division of Research Resources. Additional support of SSRL is provided by the Department of Energy, Office of Health and Environmental Research.

* Author to whom correspondence should be addressed.

‡ Departments of Medicine and Biochemistry, University of Utah Health Science Center.

§ Department of Medicinal Chemistry, University of Utah Health Science Center.

∥ Stanford University.

® Abstract published in *Advance ACS Abstracts,* July 15, 1994.

0006-2960/94/0433-9566$04.50/0

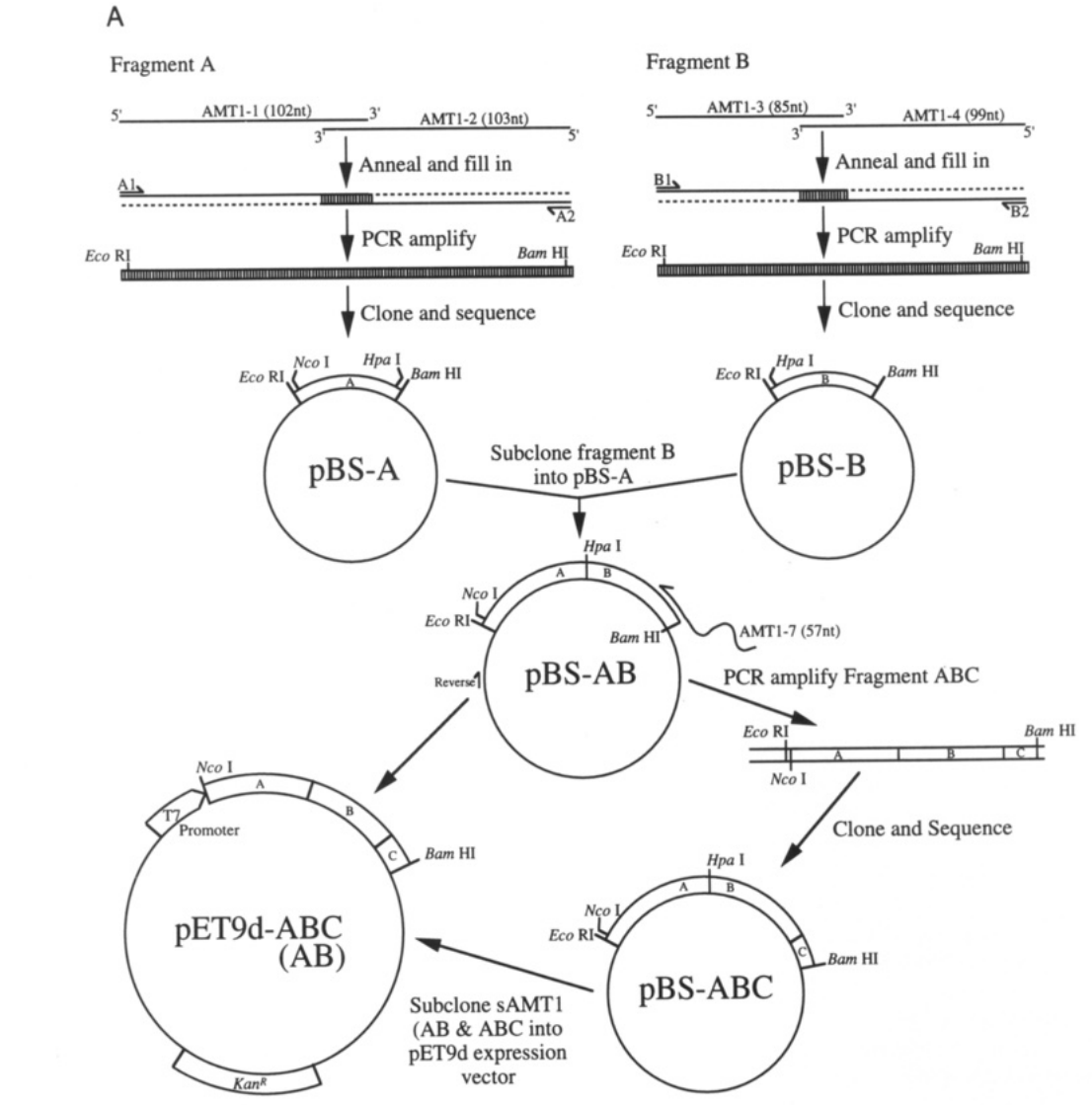

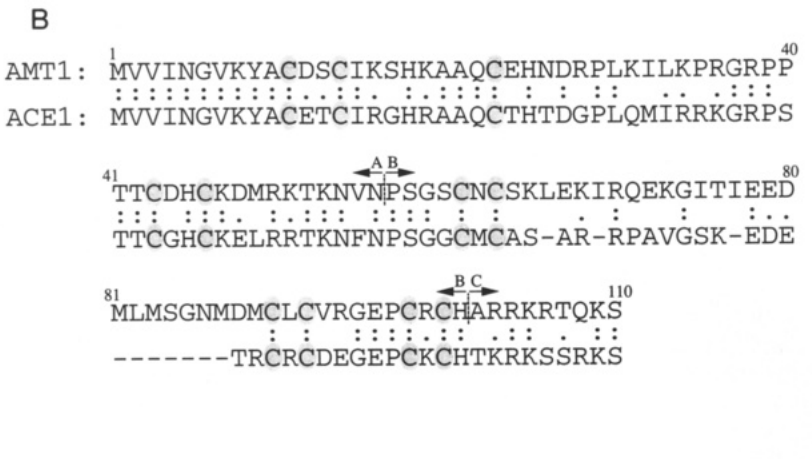

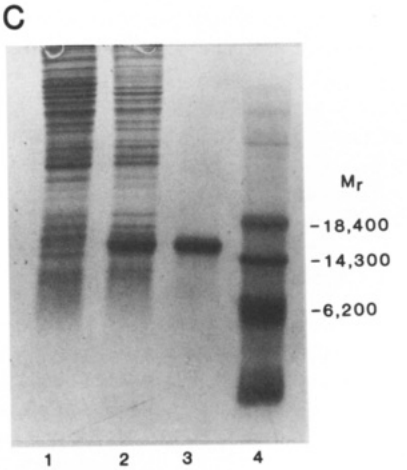

FIGURE 1: Construction of AMT1 synthetic genes and AMT1 purification. Panel A shows the schematic of the construction of the AMT1 synthetic genes. The specific oligonucleotides described in Materials and Methods, restriction enzymes, and plasmids used are illustrated. The initial fragments were cloned into pBluescript-SK, and the synthetic genes were cloned into the pET-9d expression vector. The sequence of AMT1 included in the synthetic gene is shown in panel B as well as the sequence comparison of the corresponding sequence for ACE1. The conserved cysteines, which are essential for ACE1 function (Hu et al., 1990), are shaded. The conserved sequences are indicated. The amino acids which constitute fragments A (residues 1–56), B (residues 57–101), and C (residues 102–110) of the AMT1 synthetic gene are indicated. Panel C shows the purification of Cu_4Zn_1AMT1 from *E. coli* (BL21). Extracts from cells either induced with IPTG (lane 2) or uninduced (lane 1) were electrophoresed on a SDS–polyacylamide gel. The Coomassie-stained purified AMT1 is shown in lane 3. Protein markers were electrophoresed in lane 4.

no compelling data have been reported on the pathway of cluster formation. In studies with ACE1 synthesized in a wheat germ *in vitro* system, Furst and Hamer (1989) reported cooperative binding of Cu^+ and Ag^+ ions, yet cooperativity in cluster formation has not been substantiated in biochemical studies with purified ACE1. Fourth, a paucity of information

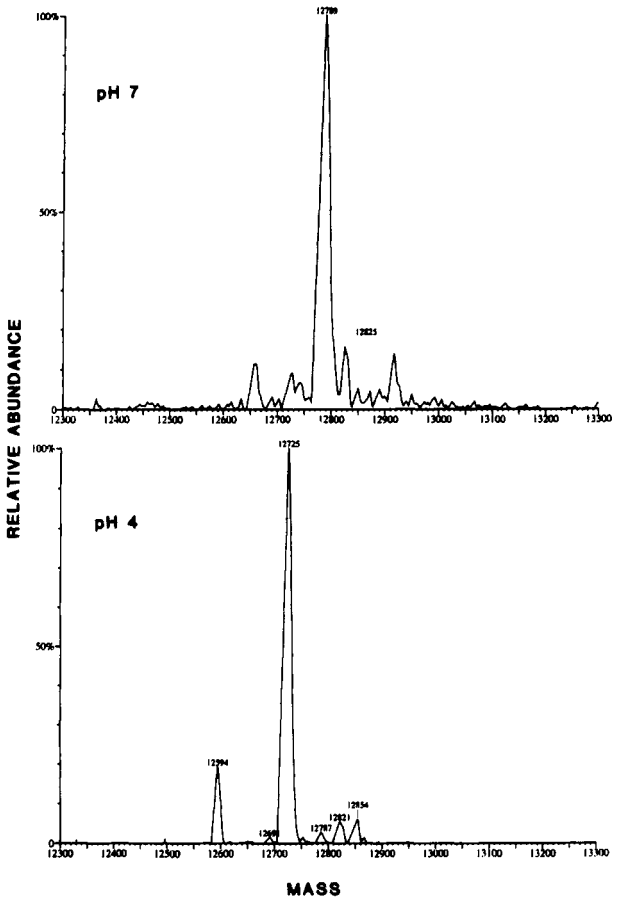

FIGURE 2: Electrospray mass spectra of Cu_4Zn_1AMT1 at pH 7.4 and 4. The pH 4 sample was prepared by acidification of the protein with acetic acid. The final acid concentration was 0.1%.

exists on how cluster formation activates the protein for specific DNA binding. Only indirect evidence has been presented that Cu^+ binding results in a conformation change in ACE1 (Furst et al., 1988).

In the present study we have purified the AMT1 DNA-binding domain with the goals of characterizing the Cu^+ sites and of later studying the interaction of AMT1 with promoter elements from the three distinct MT genes in *C. glabrata*. Evidence is presented that AMT1 forms a uniform tetracopper cluster with a nearby Zn^{2+} site and that the metal centers stabilize a unique conformation capable of sequence-specific DNA binding.

MATERIALS AND METHODS

Construction of an AMT1 Synthetic Gene. Synthetic genes were constructed for expression of the first 101 and 110 amino acids of AMT1. The genes were constructed from separate fragments designated A, B, and C (Figure 1B). Fragment A encodes amino acids 1–56, fragment B encodes residues 57–101, and fragment C encodes residues 102–110 (Figure 1B). The oligonucleotides used to construct the synthetic AMT1 genes were designed using the preferred codons for highly expressed genes in *Escherichia coli* (Andersson & Kurland, 1990). Oligonucleotides were synthesized with an ABI Model 380B DNA synthesizer. The oligonucleotides used to synthesize the AMT1 gene are as follows: AMT1-1, 5′-GCGCGGAATT CCATGGTTGT TATCAACGGT GTTAAATACG CTTGCGACTC TTGCATCAAA TCTCACAAAG CTGCTCAGTG CGAACACAAC GACCGTCCGC TG-3′; AMT1-2, 5′-GCGCGGATCC TAGTTAACGT TTTTGGTTTT ACGCATGTCT TTGCAGTGGT CGCAGGTGGT CGGCGGACGA CCACGCGGTT TCAGGATTTT CAGCGGACGG TCG-3′; AMT1-3, 5′-CGCGGGAATT CCATGGTTAA CCCGTCTGGT TCTTGCAACT GCTCTAAACT GGAAAAAATC CGTCAGGAAA AAGGTATCAC CATCG-3′; AMT1-4, 5′-GCGCGGATCC TACACGTGGC AACGGCACGG TTCACCACGA ACGCACAGGC ACATGTCCAT GTTACCAGAC ATCAGCATGT CTTCTTCGAT GGTGATACC-3′; and AMT1-7, 5′-GCGCGGATCC TAAGATTTCT GGGTACGTTT ACGACGAGCG TGGCAACGGC ACGGTTC-3′. Oligonucleotides AMT1-1 and AMT1-2 were annealed, filled in by the polymerase chain reaction (PCR), amplified, and subsequently cloned into pBluescript SK (Stratagene) to construct the fragment A duplex (Figure 1A). The annealing and filling-in reactions were accomplished using one cycle of PCR with Taq DNA polymerase (Bohringer Mannheim) with a reaction time of 5 min at 72 °C. Similarly, AMT1-3 and AMT1-4 were used to construct the fragment B duplex. The oligonucleotides used for amplification of the A and B duplexes prior to cloning were as follows: A1, 5′-GCGCGGAATTC-CATAGG-3′; A2, 5′-GCGCGGATCCTAGTT-3′; B1, 5′-CGCGGGAATTCCATGG-3′; B2, 5′-GCGCGGATCCTA-CAC-3′. The plasmids containing fragments A and B were designated pBS-A and pBS-B, respectively. The predicted sequences were confirmed by DNA sequencing with Sequenase (U.S. Biochemicals). Subsequently, fragment B was isolated from pBS-B and subcloned into pBS-A to ligate the A and B fragments in pBS-AB. Fragment C was added to fragment AB by a PCR reaction using the M13 reverse primer (Stratagene) and oligonucleotide AMT1-7 to extend the coding sequence from pBS-AB. The resulting PCR fragment was subsequently cloned into pBluescript SK and designated pBS-ABC. The predicted sequence was confirmed by DNA sequencing. Expression vectors containing the AMT1 gene were constructed by subcloning the respective fragments from pBS-AB and pBS-ABC into pET-9d (Novagen). The final vectors, designated pET9d-AB and pET9d-ABC, encode the N-terminal 101 and 110 residues of the AMT1 gene, respectively. Unless otherwise specified, standard molecular biological techniques in accordance with *Current Protocols in Molecular Biology* (Ausubel et al., 1993) were used. The construction of the plasmids, including all restriction enzymes used, is summarized in Figure 1A.

Purification of Bacterially Expressed AMT1. The AMT1 gene cloned in pET-9d was expressed in *E. coli* strain BL21 (pLysS). Cells at an OD_{600nm} of 0.5 were induced with 0.4 mM isopropyl β-D-thiolgalactopyranoside (IPTG). After 0.5 h, $CuSO_4$ was added to a final concentration of 1.4 mM and cells were incubated for an additional 2.5 h. Cells were harvested and washed with isotonic sucrose, followed by freezing at −70 °C in buffer A (10 mM sodium phosphate, pH 7.8, with 0.1 M KCl) containing 0.1% β-mercaptoethanol. Lysis was achieved by freeze–thawing followed by sonication. The extract was clarified by centrifugation at 160000*g*. The pellet was reextracted by repeated sonication of a suspension in buffer A followed by centrifugation. The combined supernatant was diluted 2-fold in 10 mM sodium phosphate, pH 7.8, followed by addition of protamine sulfate (1 mg per 5 mg of total protein). After centrifugation the supernatant was applied to a CM-cellulose column (3.2 × 8 cm) equilibrated with buffer A. Elution was achieved with a linear gradient of 0.1 to 0.4 M buffered KCl, and AMT1 eluted between 0.15 and 0.2 M KCl. Ammonium sulfate was added to the AMT1 in the eluate to a final concentration of 0.4 M,

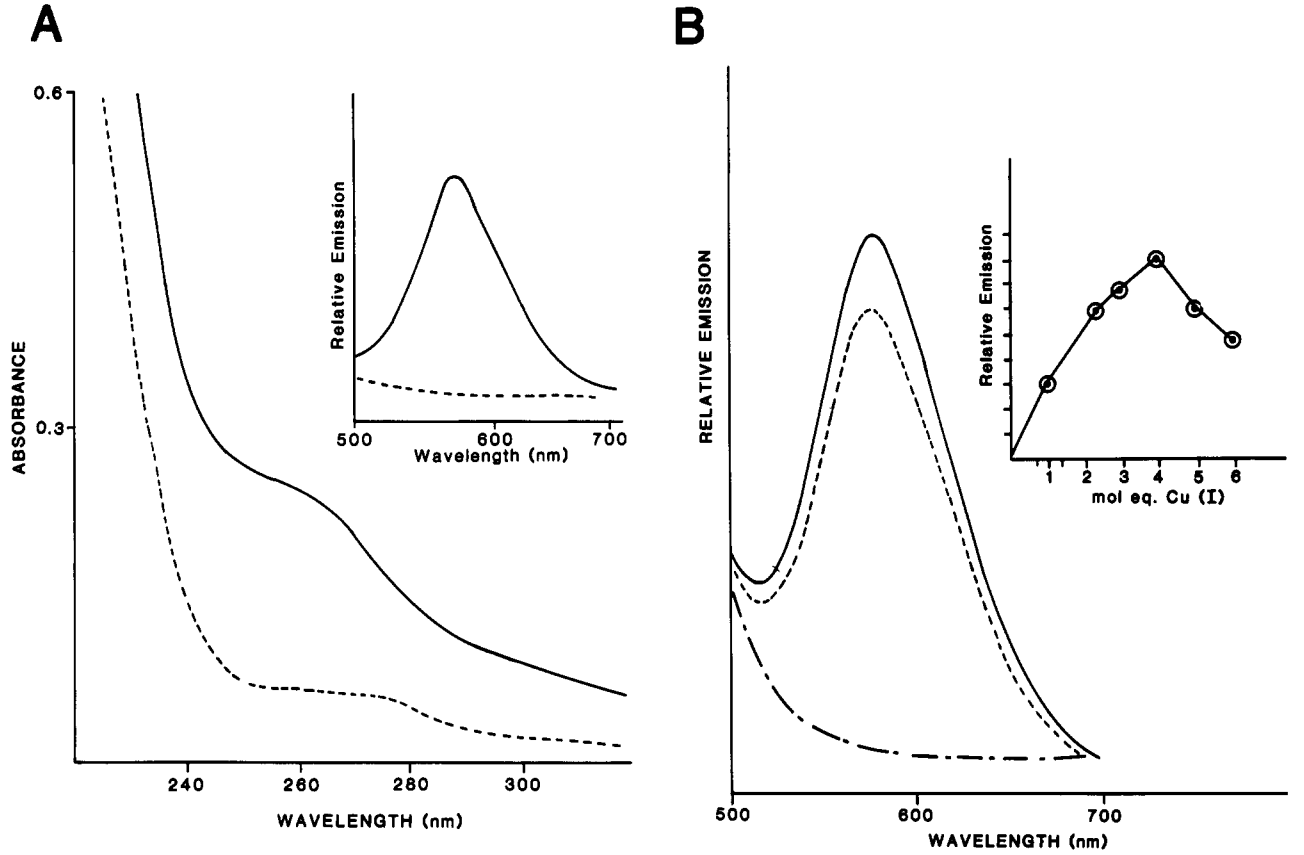

FIGURE 3: Ultraviolet absorption and emission spectra of AMT1. In panel A the ultraviolet absorption spectra of Cu_4Zn_1AMT1 (—) and apoAMT1 (- - -) are presented. Spectra of the samples were recorded at 98 μg/mL in 20 mM Tris-HCl, pH 7.4. The inset shows the uncorrected luminscence spectrum of Cu_4Zn_1AMT1 at neutral pH (—) and after acidification to pH 2 (- - -). Excitation was at 300 nm. In panel B the emission of apoAMT1 reconstituted with increasing molar equivalents of Cu^+ is shown. ApoAMT1 (2 μM) was mixed with specified amounts of Cu^+–acetonitrile at pH 2 and subsequently neutralized to pH 7.5 within an anaerobic chamber. Emission was recorded with excitation at 300 nm (titration shown in the inset). The emission spectrum of AMT1 reconstituted with 4 molar equiv is shown (- - -) and compared with an equivalent quantity of native Cu_4Zn_1AMT1 (—) and apoAMT1 (- · -).

and the fraction was applied to phenyl-Sepharose (1.6 × 3 cm) equilibrated with 0.4 M ammonium sulfate in buffer A. AMT1 was collected in the column wash, and ammonium sulfate was again added to a final concentration of 1.5 M for application to a second phenyl-Sepharose column (1.6 × 3 cm). Elution was achieved with a linear gradient of decreasing ammonium sulfate concentration from 1.5 to 0.4 M in 10 mM sodium phosphate, pH 7.8. AMT1 eluted near 1 M ammonium sulfate. DTT was added to all buffers at a final concentration of 4 mM throughout the purification protocol. AMT1 was concentrated by ultrafiltration with a YM3 (Amicon) membrane and subsequently desalted on Sephadex G-25 equilibrated with 10 mM Tris-HCl, pH 7.8. Purification of AMT1 was carried out at 4 °C, and AMT1 samples were stored anaerobically at −70 °C. Eight different isolates of AMT1 were evaluated.

Metal analysis was performed on a Perkin-Elmer 305A spectrometer. Protein was quantified by amino acid analysis following 24 h of hydrolysis in 5.7 N HCl *in vacuo* at 110 °C. Analysis was carried out on a Beckman 6300 analyzer.

ApoAMT1 was prepared by two cycles of acidification of CuZnAMT1 to a pH of 0.1 followed by gel filtration on Sephadex G-25 equilibrated with 0.025 N HCl as previously described for ACE1 (Dameron et al., 1991). The apoprotein was reduced with 150 mM DTT at neutral pH and rechromatographed on Sephadex G-25 equilibrated in 0.025 N HCl. The concentration of apoAMT1 was determined by quantitative amino acid analysis. The extent of cysteine reduction was monitored by titration with dithiodipyridine (Grassetti & Murray, 1967). ApoAMT1 samples used for Cu^+ reconstitution studies contained at least 95% of the cysteines reduced. Cu^+ reconstitution of apoAMT1 was carried out by mixing apoAMT1 at pH 2 with a predetermined molar equivalency of Cu^+–acetonitrile in an anaerobic chamber. The mixtures were neutralized with 0.2 M Tris or ammonium bicarbonate to pH 7.5–7.8.

Zn-free CuAMT1 was prepared by acidification to pH 3–4 followed by desalting on Sephadex G-25 equilibrated with 1% acetic acid. The protein concentration and metal content of the desalted sample were determined as described above. Co^{2+} reconstitution of Zn-free CuAMT1 was carried out anaerobically by mixing Zn-free CuAMT1 with a predetermined molar equivalency of Co^{2+}. The mixtures were brought to pH 8.5 with 2 M Tris.

Spectroscopic Characterization. Optical absorption spectra were recorded on a Beckman DU-65 recording spectrometer. Luminescence measurements were made on a Perkin-Elmer 650-10s fluorimeter with excitation at 300 nm. Circular dichroism spectra were recorded on an Aviv 62DS spectrometer with sample concentrations of 5 μM apoAMT1 or 19 μM Cu,ZnAMT1 in 0.1-cm cuvettes. Repetitive scans and post-run smoothing routines were used. Copper K-edge and zinc K-edge X-ray absorption spectra (EXAFS) were collected on beamline SB07-3 (1.8 T wiggler field) at the Stanford Synchrotron Radiation Laboratory. Copper K-edge and zinc K-edge data sets comprised averages of six and eight 35-min scans, respectively. During data collection, samples were maintained at a temperature close to 10°K, and X-ray absorption was measured as the X-ray fluorescence excitation spectrum using a Canberra 13-element germanium detector

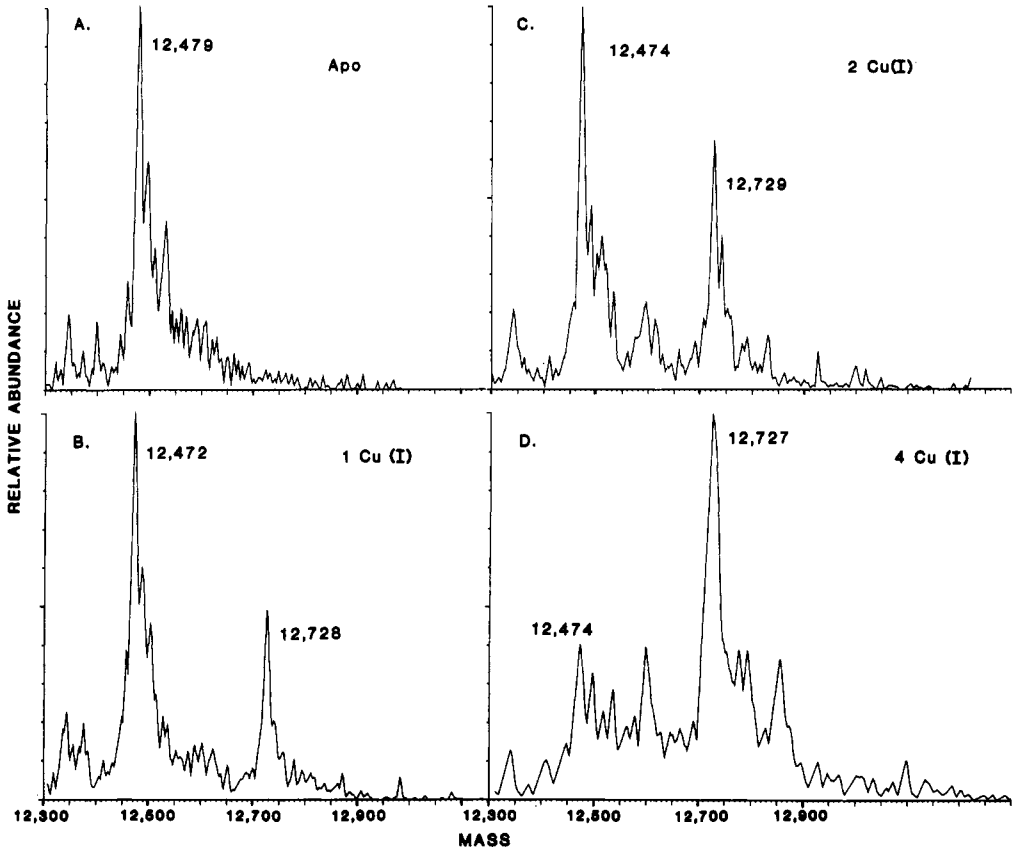

FIGURE 4: Electrospray mass spectra of apoAMT1 titrated with increasing molar equivalents of Cu^+. Panel A represents apoAMT1 at pH 2. Panels B, C, and D represent protein titrated with the equivalents of Cu^+ shown. These samples were at neutral pH. The lower apparent mass of the apo species can be accounted for by limited oxidation of cysteinyl thiolates.

(Cramer et al., 1988). All other experimental conditions and EXAFS data analysis procedures were as previously described (Pickering et al., 1993).

Electrospray Mass Spectrometry of AMT1. The proteins were analyzed by electrospray mass spectrometry on a Fisons Instruments Trio 2000 mass spectromoter (VG Biotech, Cheshire, U.K.). The instrument data system consisted of an IBM-compatible PC which ran the LAB BASE software provided with the mass spectrometer. Typical instrument operating conditions were as follows: probe potential, 2.30 kV; counter electrode potential, 0.25 kV; sampling cone potential, 46 V. The instrument was scanned from m/z 700 to 1700 at a rate of 10 s per scan, and 10–25 scans were summed to obtain each spectrum. After acquisition, the spectra were smoothed and the baseline was subtracted. Transformed spectra were obtained using the subroutine provided with the LAB BASE software.

The metalloprotein samples were analyzed in 5–20 mM buffer (ammonium bicarbonate or Tris) at concentrations of 10–100 μM. The pH of the solutions was adjusted as necessary using glacial acetic acid. The apoprotein, unless stated otherwise, was analyzed with 10% glacial acetic acid by volume. The resulting solutions were infused into the mass spectrometer at a rate of 4–6 μL/min using a Harvard syringe pump (South Natick, MA).

AMT1–DNA Binding. Oligonucleotides spanning the AMT1 binding site of the AMT1 gene (Zhou et al., 1992) were synthesized with an ABI 380B DNA synthesizer. The oligonucleotides were pAMT1t (5′-TCATGATAAG-CTAATTTGGCTGACT-3′) and pAMT1b (5′-AAGT-CAGCCAAATTAGCTTATCATG-3′). pAMT1t and pAMT1b were gel isolated from an 18% polyacrylamide gel and then desalted on Sephadex G-25 equilibrated in 10 mM Tris-HCl, pH 7.8. Equimolar concentrations of each oligonucleotide were end-labeled with ^{32}P and then annealed.

Gel shift reactions were performed by incubating AMT1 with labeled duplex DNA in the presence of 65 mM KCl, 0.1 mg/mL dog serum albumin (DSA), 10% glycerol, 5 mM $MgCl_2$, and 20 mM Tris-HCl, pH 7.8. Some experiments, as specified, included 1 mM DTT or 3 mM EDTA in the reaction mix. After incubation at room temperature for 15 min, reaction mixtures were applied to 6% (preelectrophoresed) polyacrylamide gels in 1× TBE and electrophoresed at 200 V for 1.5–2 h at room temperature. Concentrated apoAMT1 was neutralized to pH 7.8 by dilution in 20 mM Tris-HCl, pH 7.8. Concentrated Cu,ZnAMT1 was used to prepare Zn-free CuAMT1 by reducing the pH to 4 with acetic acid followed by the addition of EDTA and neutralization to pH 7.8, to chelate liberated Zn^{2+} ions.

RESULTS

Construction of an AMT1 Synthetic Gene. A synthetic gene for the DNA-binding domain of AMT1 was constructed, as the wild-type AMT1 gene was poorly expressed in *E. coli*. The design of the synthetic gene involved optimizing the codon bias for *E. coli* without changing the AMT1 protein sequence. Two genes were constructed, one encoding residues 1–101 and the other encoding residues 1–110 (Figure 1A). Each was cloned into pET9d, and they were designated pET9-AB and pET9-ABC, respectively. These segments of the AMT1 protein exhibit a 50% sequence identity with the ACE1 protein from *S. cerevisiae* (Figure 1B).

Purification of AMT1. Expression of the DNA-binding domain of AMT1 was induced by IPTG from vectors pET9-AB and pET9-ABC in *E. coli*. The respective 101- and 110-

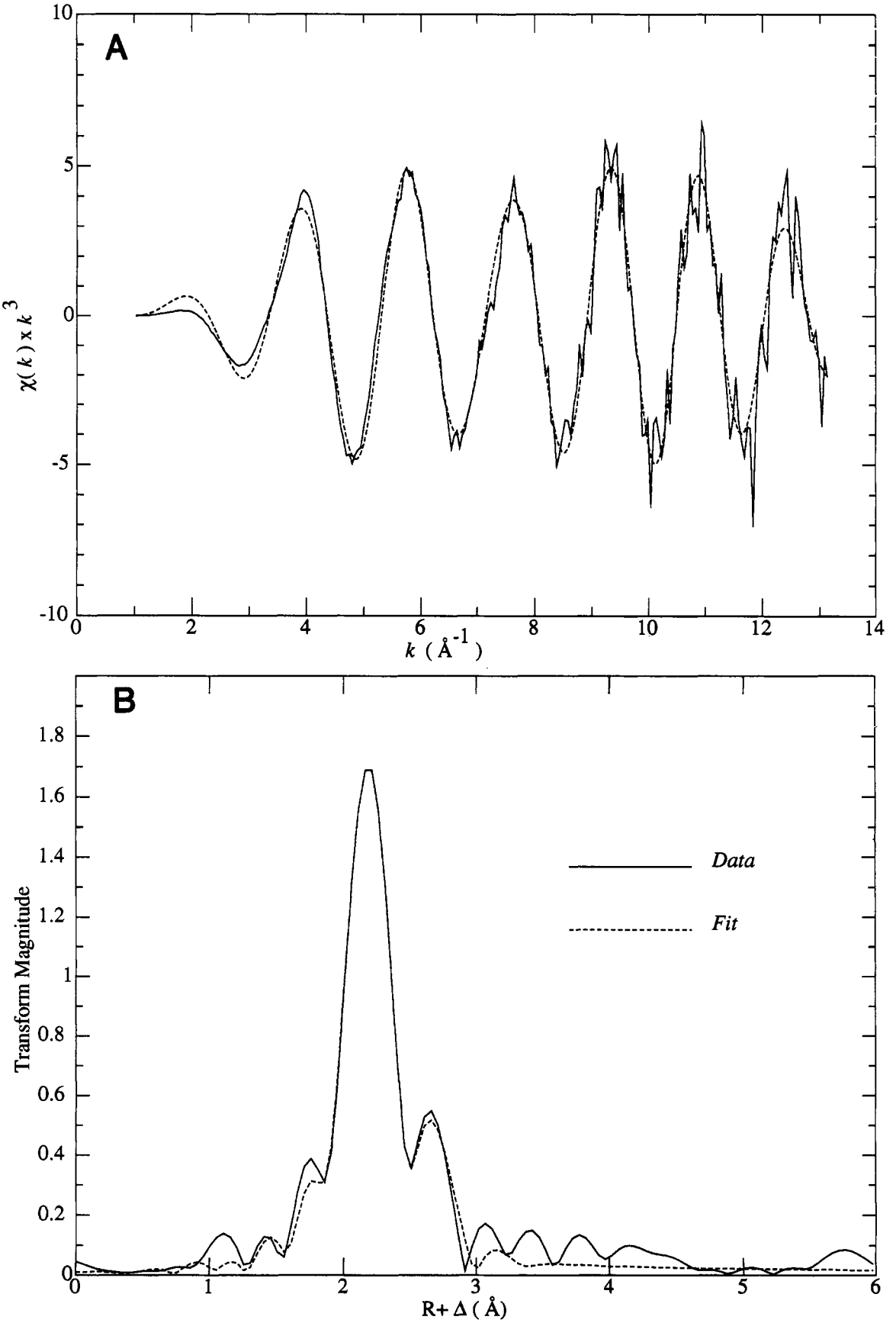

FIGURE 5: Cu K-edge EXAFS analysis of Cu_4Zn_1AMT1. Panels A and B show the EXAFS and Fourier transform, respectively. The solid lines show the κ^3-weighted raw EXAFS data, and the dashed lines, the results of the fit as shown in Table 1.

residue polypeptides were visible on a Coomassie-stained SDS–polyacrylamide electrophoresis gel (Figure 1C, lane 2, for pET9-ABC). However, the 110-residue AMT1 appeared to be expressed at higher levels than the 101-residue protein (data not shown). Consequently, pET9-ABC was used for expression of AMT1 for purification.

AMT1 was purified from bacterial cells expressing AMT1 from pET9-ABC in the presence of added $CuSO_4$. It was

Table 1: EXAFS Curve-Fitting Results of Cu_4Zn_1AMT1[a]

shell	N	R (Å)	σ^2 (Å^2)	F_{fit}[b]
Cu–S	3.0	2.263 (4)	0.0038 (5)	0.5474
Cu–Cu	1.0	2.745 (14)	0.0054 (16)	
Zn–S	4	2.306 (11)	0.0075 (07)	0.9261
Zn–Cu	1	3.535 (32)	0.0062 (33)	

[a] The phase and amplitude functions used in the fit were as described previously (Pickering et al., 1993). Coordination numbers were chosen to give the best fit to the nearest ±0.2 for Cu–S, the nearest ±0.5 for Cu–Cu, the nearest integer for first shell Zn, and the nearest ±0.5 for outer shell scatterers. The precision, in the form of estimated 95% confidence limits (obtained from the diagonal elements of the covariance matrix), is given in parentheses for each of the parameters floated in the fit. It should be noted that the accuracy of the EXAFS-derived structural parameters will be poorer than this, probably ±0.02 Å for R and ±25–30% for N and σ^2 [see Pickering et al. (1993) for a more complete discussion]. Values of E_o, the offset to the energy zero, were chosen as in the previous work (Pickering et al., 1993). [b] Goodness of fit parameter, defined as $F_{fit} = (\Sigma(\chi_o - \chi_c)^2k^6)/(\eta_{obs} - \eta_{var})$, where χ_o and χ_c are the observed and calculated EXAFS, respectively (κ^3-weighted), and η_{obs} and η_{var} are the number of observations and variables floating in the refinement, respectively.

recovered in the soluble protein fraction. Protamine sulfate was added to the clarified extract to remove nucleic acids, and the resulting supernatant was chromatographed on CM-cellulose, phenyl-Sepharose, and a final Sephadex G-25 column for desalting. The assays used to monitor the presence of AMT1 during purification included copper and zinc analyses, luminescence, and SDS–polyacrylamide gel electrophoresis. Approximately 2–4 mg of AMT1 was isolated per liter of culture.

AMT1 was shown to be homogeneous by four criteria. First, a single band of apparent M_r 15 500 was observed on a stained SDS–polyacrylamide gel (Figure 1C, lane 3). Second, amino acid analysis after acid hydrolysis revealed an amino acid composition identical to that predicted from the nucleotide sequence of residues 1–110. Third, in the first two cycles, the Met-Val sequence accounted for >90% of the total picomoles of phenylthiohydantoin-derivatized amino acids in the chromatogram. Val was observed in cycle 1 at approximately 25% of the Met yield, consistent with the presence of limited amounts of the desMet form of AMT1. Fourth, electrospray mass spectrometry of the metal-depleted AMT1 revealed a predominant species of 12 478 ± 1 Da. This mass was in excellent agreement with the mass calculated from the decoded nucleotide sequence (12 479 Da). The presence of a minor desMet AMT1 species was indicated by the small component of 131 amu less than expected. Thus, the major AMT1 species consists of 110 residues.

The apparent M_r from SDS electrophoresis of 15 500 significantly exceeds the actual M_r (12 478) as determined by mass spectrometry. This may be explained by the basic nature of AMT1. AMT1 chromatographed on Superose G-75 with an apparent M_r of 20 000 consistent with the AMT1 fragment being monomeric with limited asymmetry in hydrodynamic properties.

Metal Content of AMT1. Metal analysis of AMT1 revealed the presence of copper and zinc. Mean contents of copper and zinc of 4.2 ± 0.2 (n = 8 different isolates) and 1.2 ± 0.2 (n = 8), respectively, were observed.

Electrospray MS was carried out on the purified Cu,ZnAMT1 to assess the uniformity of the metal centers in AMT1. Electrospray MS has been shown to be effective in characterizing noncovalent interactions, including metal–protein interactions (Hutchens & Allen, 1992; Allen & Hutchens, 1992; Yu et al., 1993).

Analysis of two different samples at neutral pH revealed a mass spectrum of the metallated AMT1. One major species of mass 12 789 Da was observed, consistent with five metal ions (Cu + Zn) bound (Figure 2). The accuracy of mass measurements is limited in part by the uncertainty in the number of cysteine residues present as ionized thiolates. The minor component at mass 12 658 Da is likely to be the metallated desMet form of AMT1. Analysis of AMT1 diluted in 0.1% acetic acid to pH 4 yielded a mass spectrum with a major species at 12 725 Da, consistent with the loss of the labile Zn^{2+} ion. Again, the minor component at mass 12 594 Da is likely to be the desMet form of AMT1. Chromatography of native AMT1 on Sephadex G-25 equilibrated at pH 4 resulted in the recovery of AMT1 lacking the bound Zn^{2+} ion but retaining the 4 Cu^+ ions.

Analysis of the Copper Sites in AMT1. All AMT1 isolates exhibited transitions in the ultraviolet consistent with S → Cu charge-transfer bands (Figure 3A). AMT1 exhibited orange luminescence when excited with ultraviolet light (Figure 3A, inset). Emission occurred at 575 nm, and an excitation maximum was seen near 300 nm. The luminescence is indicative of the bound copper being present as Cu^+ (Lytle, 1970).

To verify that maximal Cu^+ binding occurred at 4 molar equiv, Cu^+ reconstitution studies were carried out with AMT1 depleted of bound metal ions. ApoAMT1 was prepared by gel filtration at low pH. After reduction of the 11 cysteinyl residues in apoAMT1, the apoprotein was titrated with increasing quantities of Cu^+ stabilized as Cu^+–acetonitrile and the emission was quantified. Emission was maximal at 4 molar equiv of added Cu^+ in multiple reconstitution experiments (Figure 3B, inset). The relative quantum yield of emission of Cu-reconstituted AMT1 was similar to that of purified Cu,ZnAMT1 (Figure 3B). As with CuACE1 and Cu-metallothioneins, the Cu^+ emission in the CuAMT1 complex was quenched by oxygen and diminished in a concentration-dependent manner with excess Cu^+ (data not shown).

To determine whether Cu^+ binding occurred in an all-or-nothing manner, apoAMT1 was titrated with increasing quantities of Cu^+ ranging from 1 to 4 molar equiv followed by electrospray MS to detect the metallated species (Figure 4). The mass spectrum of AMT1 after addition of 1 molar equiv Cu^+ to apoAMT1 yielded two components. The major species had a mass identical to that of apoAMT1. The second component of mass 12 728 ± 1 amu was consistent with a tetracopper AMT1 species. Mass spectrometry of AMT1 reconstituted with 2 molar equiv Cu^+ yielded the same two components but with an increased abundance of the tetracopper species. Analysis of AMT1 reconstituted with 4 molar equiv Cu^+ revealed only the tetracopper species. There was no indication of AMT1 molecules with lower integer levels of metallation. The addition of various ions to achieve neutral pH and Cu^+ reconstitution resulted in a myriad of minor peaks.

X-ray absorption spectroscopy was carried out to probe the structure of the copper sites in AMT1. The copper K absorption edge showed a feature at 8983 eV arising from a 1s → 4p transition of Cu^+ (data not shown). The intensity of the edge feature is similar to that observed with trigonal Cu^+ complexes, although the presence of digonal Cu^+ coordination in Cu–thiolate clusters cannot be excluded from edge data (Pickering et al., 1993).

Extended X-ray absorption fine structure (EXAFS) spectroscopy revealed more detailed information about the local

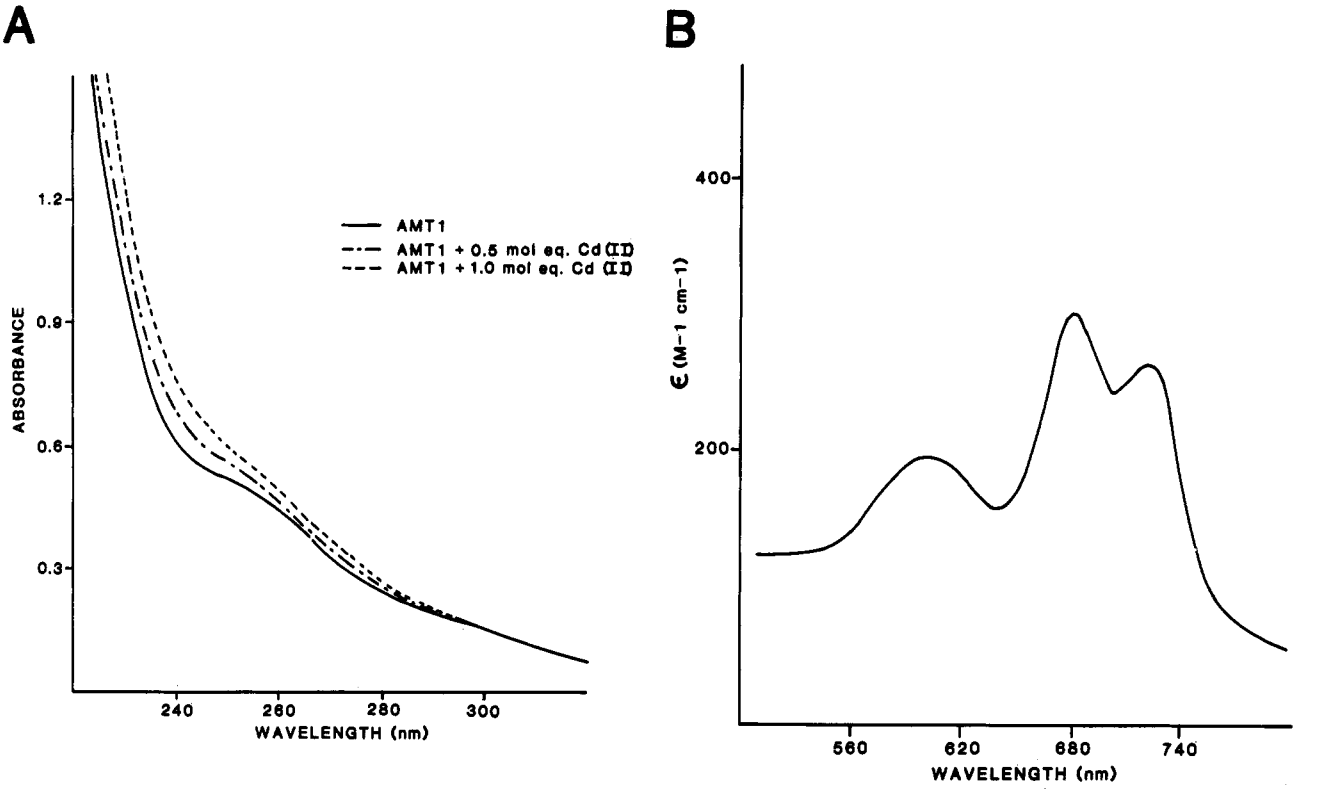

FIGURE 6: Analysis of the Zn^{2+} site in AMT1. Panel A shows the Cd^{2+} displacement of Zn^{2+} in Cu_4Zn_1AMT1. Samples of AMT1 were titrated with increasing quantities of Cd^{2+} at neutral pH. Panel B shows the electronic spectrum of the Co^{2+} complex of AMT1, Cu_4Co_1AMT1, prepared by the addition of 1.2 molar equiv Co^{2+} to Zn-free Cu_4AMT1 and subsequent adjustment of the pH to 8.5.

Cu^+ environment. The copper K-edge EXAFS spectrum and corresponding Fourier transform shown in Figure 5 are dominated by a first shell scattering peak that was best fit with Cu–S bonding (Table 1). The bond length determined from a curve-fitting analysis of the EXAFS oscillations was 2.26 Å, which is consistent with predominantly trigonally coordinated copper, although a small fraction (ca. 25%) of digonal copper may be indicated by this mean Cu–S bond length (see Pickering et al., 1993). A second, smaller scatterer peak in the Fourier transform is also seen. This fits well to a Cu–Cu interaction at 2.75 Å, indicating the presence of a polycopper cluster. The mean number of Cu^+ scatterers per Cu atom (N in Table 1) was 1, unlike the value of 3 for the synthetic Cu_4S_6 cage clusters (Pickering et al., 1993).

Analysis of the Zn^{2+} Site in AMT1. Electronic spectroscopy was carried out on samples in which Cd^{2+} or Co^{2+} was substituted for the bound Zn^{2+} ion in AMT1 to probe the coordination environment of the Zn^{2+} ion. The addition of exogenous Cd^{2+} resulted in the displacement of AMT1-bound Zn^{2+} and the appearance of cysteinyl S → Cd charge-transfer bands in the ultraviolet (Figure 6A). The S → Cd charge-transfer band was maximal at 1 molar equiv of added Cd^{2+}.

Co^{2+} is frequently used as a spectroscopic probe of Zn^{2+} sites in metalloproteins (Bertini & Luchinat, 1984). Zn-depleted CuAMT1 was prepared by gel filtration at pH 4 resulting in a Cu_4AMT1 species. Zn-depleted Cu_4AMT1 was reconstituted with 1 molar equiv Co^{2+} (Figure 6B). The resulting sample at pH 8.5 exhibited d–d transitions with maxima at 616 [ϵ = 196 $M^{-1}cm^{-1}$], 682 [ϵ = 298 M^{-1} cm^{-1}], and 737 nm [ϵ = 261 M^{-1} cm^{-1}]. The energy of these transitions and the molar extinction coefficients are typical of $\nu_3[^4A_2 \rightarrow {}^4T_1(P)]$ transitions of four-coordinate high-spin Co^{2+} complexes having distorted tetrahedral coordination geometry (Lane et al., 1977; Swenson et al., 1978; Dance, 1979; Johnson & Schachman, 1983; Bertini & Luchinat, 1984; Giedroc & Coleman, 1986). The molar extinction coefficient of the d–d transitions of tetrahedral Co^{2+} complexes is typically 250–1000 M^{-1} cm^{-1} per Co^{2+} ion. The energy of the d–d envelope is consistent with either S_4 ligation or mixed sulfur/nitrogen ligation. Tetrathiolate Co^{2+} complexes exhibit a prominent transition between 730 and 760 nm. This low-energy band is not seen in complexes with a nitrogen ligand. The presence of a shoulder transition at 730 nm in Cu_4Co_1-AMT1 is consistent with tetrathiolate coordination (Maret et al., 1979; Geidroc & Coleman, 1986; Xu et al., 1993; Michelsen et al., 1994).

The zinc K-edge EXAFS and the corresponding EXAFS Fourier transform are shown in Figure 7. Curve-fitting analysis of the EXAFS indicates that the spectrum is dominated by a first coordination shell of Zn–S at about 2.31 Å, giving rise to the pronounced transform peak at $R + \Delta$ = 2.3 Å. The first shell can be fit either by four Zn–S interactions or by three Zn–S interactions plus a single lighter scatterer (oxygen or nitrogen). The EXAFS fit is slightly improved when the ZnS_3N_1 coordination is used (data not shown). The Zn–(O/N) distance of about 2.02 Å yields EXAFS which is in phase with the Zn–S EXAFS and so is very difficult to distinguish. A smaller peak in the transform at $R + \Delta$ = 3.7 Å is also visible in the EXAFS Fourier transform. EXAFS curve fitting shows that this feature fits well to a single Zn–Cu interaction at about 3.54 Å. However, this feature could also be fit (although marginally less adequately) to Zn–C at a similar distance. The amplitude function is more consistent with a Zn–Cu interaction. Curve fitting of this outer shell EXAFS using a full multiple scattering treatment for Zn–histidine ligation did not fit the data, and we conclude that no such ligation is present. In the absence of Zn–histidine coordination, we conclude that the Zn^{2+} site is likely to have tetrathiolate coordination.

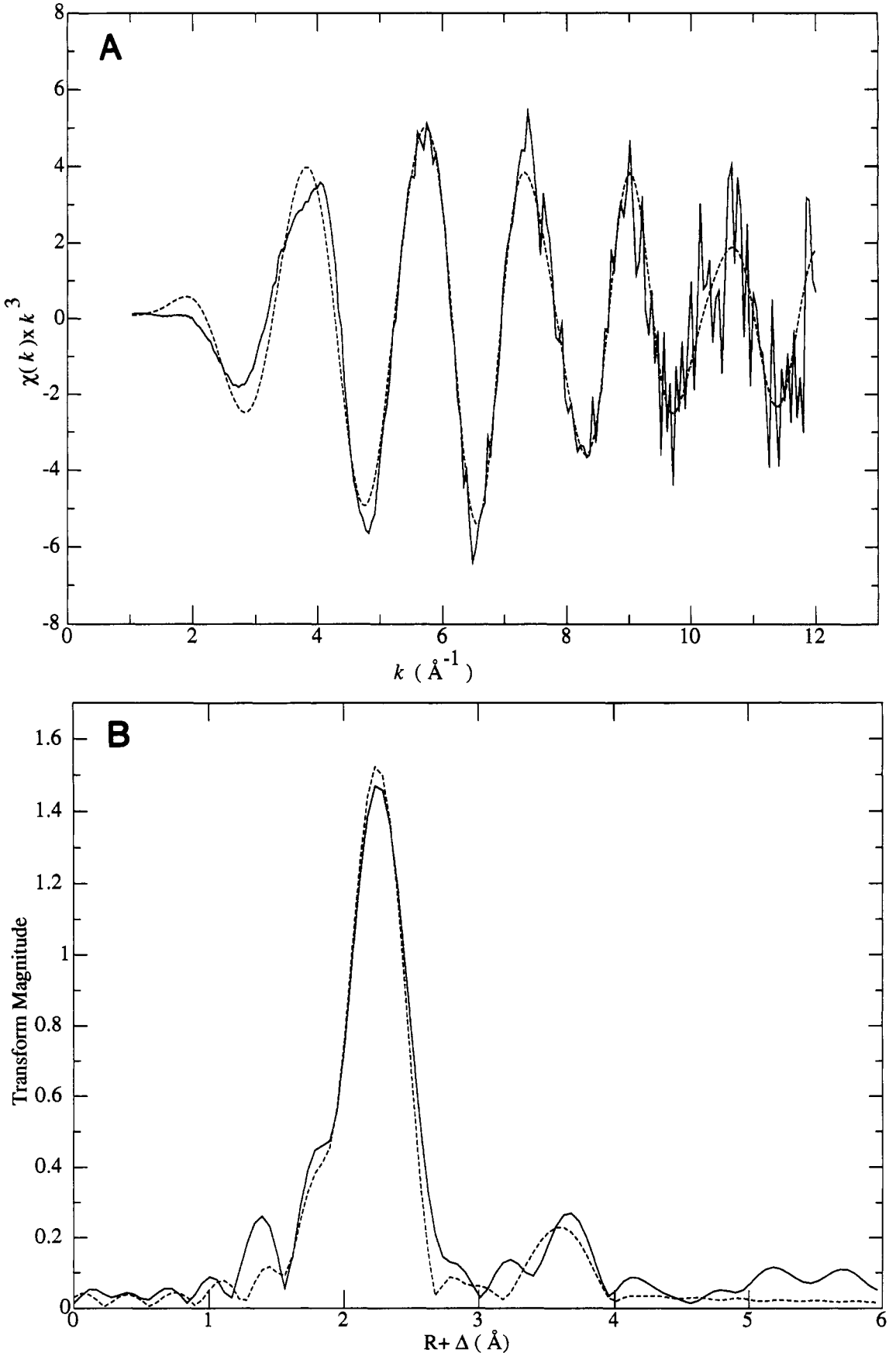

FIGURE 7: Zn K-edge EXAFS analysis of Cu_4Zn_1AMT1. Panels A and B show the EXAFS and Fourier transform, respectively. The solid lines show the κ^3-weighted EXAFS data, and the dashed lines, the results of the fit as shown in Table 1.

Role of Metal in AMT1 Structure. Circular dichroism (CD) studies were carried out to determine whether the tertiary fold of native AMT1 was influenced by Cu^+ binding. A comparison of Cu_4Zn_1AMT1 to apoAMT1 revealed attenuated ellipticity in the metal-free molecule consistent with a loss of periodic secondary structure (Figure 8). Computer

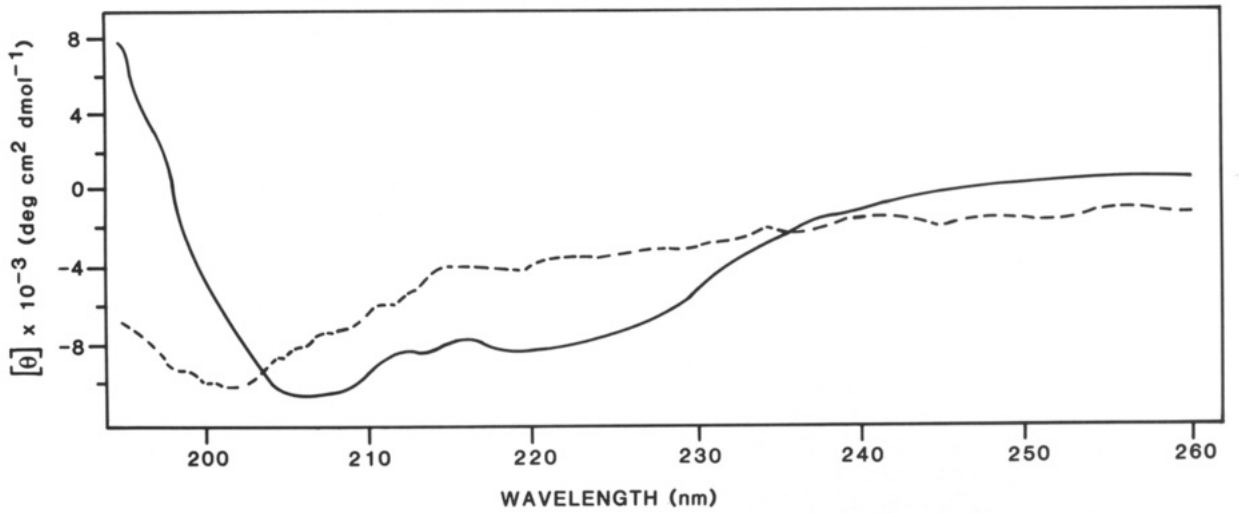

FIGURE 8: Circular dichroism of Cu_4Zn_1AMT1 and the metal-depleted AMT1 protein. The ellipticity spectra of metalloAMT1 (—) and apoAMT1 (- - -) were measured in 10 mM Tris-HCl, pH 7.4. The spectra represent an average of three scans with a bandwidth of 0.7 nm.

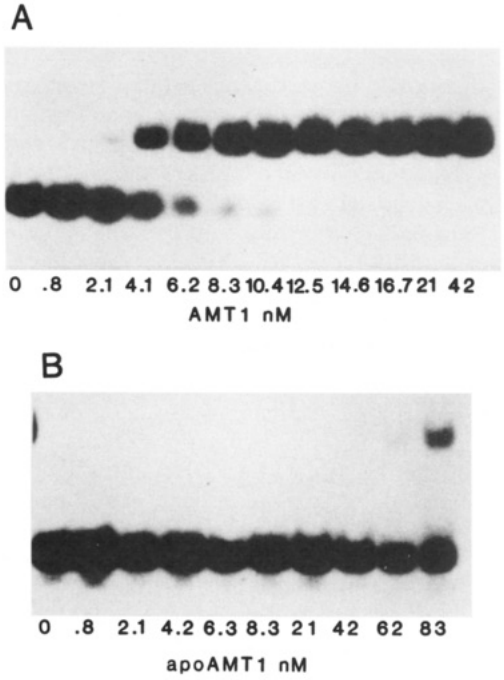

FIGURE 9: Gel shift analysis of Cu_4Zn_1AMT1 (panel A) and apoAMT1 (panel B). Protein was mixed with a labeled DNA duplex containing the AMT1 upstream activation sequence as described in Materials and Methods. The incubation conditions for both proteins included 1 mM DTT. The numbers refer to the final concentration of protein.

analysis of the CD spectra of Cu_4Zn_1AMT1 suggested the presence of both α and β structural elements; these structural elements were diminished in the apoAMT1 molecule.

Role of Metal in AMT1–DNA Binding. The role of the Cu^+ center in the DNA-binding function of AMT1 was evaluated by gel retardation assays using a 25-bp DNA oligonucleotide sequence consisting of the single AMT1 promoter element upstream of the AMT1 gene (Zhou & Thiele, 1993). Gel shift assays were carried out with varying concentrations of Cu_4Zn_1AMT1 and apoAMT1 at pH 7.8. The concentration of metallated AMT1 required for shifting 50% of the labeled DNA probe was near 6 nM (Figure 9A). In contrast, a significant band shift was seen with apoAMT1 only at concentrations in excess of 80 nM (Figure 9A). Copper analysis of apoAMT1 showed that the upper limit of Cu_4-AMT1 present in the apoAMT1 preparation was about 1%, so the band shift observed with the apoAMT1 preparation may arise from residual metallated AMT1. Specificity in DNA binding was demonstrated by the lack of any gel shift of a DNA probe consisting of the Ets1 DNA binding site (data not shown) (Nye et al., 1992).

Gel shift analysis was carried out on CuAMT1 devoid of Zn^{2+} to determine whether occupancy of the Zn^{2+} site was important in DNA binding. It was determined by varying the concentrations of Zn-free CuAMT1 in the gel shift assay that the apparent binding affinity was comparable to that of the Cu_4Zn_1AMT1 complex (or slightly inhibited) (data not shown). Whereas Zn^{2+} removal did not significantly affect DNA binding, the Zn-free CuAMT1 formed a complex with DNA exhibiting reduced electrophoretic mobility.

DISCUSSION

AMT1 is the transciption factor in *C. glabrata* that mediates the Cu-induced expression of MT genes (Thiele, 1992). The Cu-induced expression occurs by Cu-dependent activation of AMT1 yielding a conformer that is competent to bind to DNA promoter sequences upstream of MT genes. We show in this report that a uniform species of Cu_4Zn_1AMT1 was purified from the soluble protein fraction of bacteria grown in copper salts. The pure Cu_4Zn_1AMT1 complex bound DNA in a sequence-specific manner forming a high-affinity complex. Thus, the results imply that the Cu-activated conformer of AMT1 consists of a tetracopper center and an isolated Zn^{2+} site that together stabilize a specific tertiary fold.

Zn^{2+} was not previously analyzed in bacterially expressed ACE1 (Dameron et al., 1991; Nakagawa et al., 1991). *In vitro* Cu^+ reconstitution studies showed maximal Cu^+ binding at 6 molar equiv, although the binding studies were typically biphasic with an inflection point at 4 molar equiv. We have preliminary evidence that using the purification protocol described here for AMT1 to purify ACE1 results in the isolation of ACE1 with four Cu^+ ions and a single Zn^{2+} ion bound. The variable Cu^+ stoichiometry reported previously (Dameron et al., 1991) may have arisen from inadequate cell washing from culture media containing 1 mM $CuSO_4$.

The observation of Zn^{2+} in bacterially expressed AMT1 raises the question of whether AMT1 in yeast would, likewise, contain bound Zn^{2+}. A number of observations suggest that AMT1 may indeed contain Zn^{2+} in yeast. First, AMT1 was invariably isolated with a bound Zn^{2+} ion from bacteria cultured in the presence of 1.4 mM $CuSO_4$. Second, Cu^+ reconstitution studies did not reveal Cu^+ ions bound in excess

of 4 molar equiv. Third, our preliminary data suggests that the Zn^{2+} ion in AMT1 is not displaced by Cu^+. Our results are suggestive, but do not prove, that the metal content of bacterially isolated AMT1 is the physiological metal ion content.

The Cu^+ sites in AMT1 appear to be clustered, as shown by the short Cu–Cu scatter distance in EXAFS of Cu_4Zn_1-AMT1. There is no direct proof that all four Cu^+ ions exist within the same polycopper cluster, but there is chemical precedence for a Cu_4S_6 cluster. Tetracopper Cu_4S_6 cage clusters have been repeatly observed in Cu^+ complexes with small thiolate ligands [reviewed in Dance (1986) and Dance et al. (1992)]. The synthetic Cu_4S_6 clusters contain Cu^+ ions in trigonal coordination geometry with distortion from planarity (Dance, 1986). Features of the synthetic tetracopper clusters include a mean Cu–S bond distance of 2.27 Å and short 2.7-Å Cu–Cu distances (Dance et al., 1983; Nicholson et al., 1985; Dance, 1986). The clusters are held together by bridging thiolates (Dance, 1986). Cu–Cu bonding is a minor energetic factor in the stability of the clusters. The similarity in Cu–S bond distances and Cu–Cu distances in Cu_4Zn_1-AMT1 and synthetic Cu_4S_6 cage clusters is consistent with the four Cu^+ ions in AMT1 being clustered. However, the weak Cu–Cu scattering as shown by the low N value for the Cu–Cu scatter interaction may either imply that not all four Cu^+ ions exist within the same cluster or alternatively that deviations from ideality exist within a tetracopper cluster. A definitive interpretation cannot be made, but two observations provide an argument for the interpretation of a single distorted tetracopper cluster. First, the all-or-nothing formation of a tetracopper complex is consistent with a single CuS cluster. Second, the Cu–Cu scatter interaction observed in yeast Cu-metallothionein that forms a single Cu_7S_{10} cluster showed N values of 0.5 and 1.5 for two distinct samples (Pickering et al., 1993). Thus, biological CuS clusters may show prominent distortions from the known synthetic symmetrical cage clusters (Dance, 1986).

The Zn^{2+} site in AMT1 contains thiolate ligands as demonstrated by electronic spectroscopy of Cu_4Cd_1AMT1 and Cu_4Co_1AMT1. The center of the d–d envelope near 680 nm rules out complexes with two or fewer thiolates. A Co^{2+} complex with S_2N_2 coordination was shown to have the centroid of the d–d envelope near 600 nm (Mastropaolo et al., 1977). The observation of the d–d transition at 730 nm in the Co-containing AMT1 is consistent with tetrathiolate coordination. Such low-energy transitions have been observed only in Co^{2+}–protein complexes with exclusive thiolate ligation (Dance, 1979; Maret et al., 1979; Bertini & Luchinat, 1984; Fitzgerald & Coleman, 1991; Giedroc et al, 1992; Michael et al., 1992; Xu et al., 1993; Kosa et al., 1994). Zn K-edge EXAFS is also consistent with S_4 ligation. We were unsuccessful in confirming a tetrathiolate site by ^{113}Cd NMR spectroscopy, as no signal was observed in two samples of Cu_4Cd_1AMT1.

Cu_4Zn_1AMT1 may consist of a Cu_4S_{6-7} cage cluster and a distinct ZnS_4 site or alternatively a novel Cu_4Zn–thiolate mixed metal cluster. The outer shell scatter peak in the Zn EXAFS is suggestive, but not proof, of a Zn–Cu distance of 3.5 Å. If this short Zn–Cu interaction can be verified, then the Zn^{2+} site may be part of a novel Cu_4Zn_1–thiolate mixed metal cluster. All cysteinyl residues in ACE1 corresponding to the 11 in AMT1 have been shown to be essential for function (Hu et al., 1990). The presence of thiolate ligands for Zn^{2+} binding in AMT1 indicates that not all 11 cysteinyl residues are involved in Cu^+ binding. Results indicate that Zn^{2+} is bound by three or four thiolates; therefore, the Cu^+ cage cluster would contain no more than eight Cys thiolates. If more than six cysteinyl residues are involved in a single Cu^+ cluster, the implication is that not all thiolates would be doubly bridging as in the synthetic tetracopper cage (Dance, 1986).

The ability of AMT1 to bind DNA is dependent on formation of the CuS cluster. This is consistent with the known dependency of MT gene transcription on the copper concentration in the culture medium (Hamer, 1986; Furst et al., 1988). The Cu-induced conformer of AMT1 must exhibit the proper juxtaposition of residues for DNA contact. Mapping of the AMT1 binding site within the *AMT1* promoter region revealed a DNaseI footprint extending over 26 bp (Zhou & Thiele, 1993). Analysis of the AMT1–DNA complex by methylation interference revealed that a number of G and A bases within an 8-bp segment are critical for complex formation (Zhou & Thiele, 1993). The implication is that the tetracopper cluster stabilizes a conformer capable of both major and minor groove contacts. The DNA contacts in ACE1 appear to extend over one and one-half turns of a B-form DNA helix such that the protein will likely make base-specific contacts with the major groove at the two ends of the promoter sequence and span the minor groove near the middle (Buchman et al., 1990). The magnitude of structural change induced by formation of the tetracopper cluster must extend over significant portions of the AMT1 and ACE1 molecules. The differences in ellipticity in apoAMT1 and Cu_4Zn_1AMT1 by circular dichroism are consistent with a major structural change. The ellipticity change observed may reflect secondary structure changes or chirality due to the Cu^+ center. Since no chirality is observed from the polycopper clusters in metallothionein (Dameron et al., 1991), we conclude that the ellipticity change arises from secondary structure changes.

The lack of an observed effect of the Zn-free AMT1 complex in the DNA binding gel retardation assay does not imply that Zn^{2+} binding is unimportant in function. Occupancy of the Zn^{2+} site in AMT1 may not affect DNA interaction directly but may be critical for the transcriptional activation function in AMT1. Alternatively, removal of AMT1-bound Zn^{2+} may not appreciably alter DNA binding affinity but may alter the pattern of AMT1–DNA contacts. Hg^{2+} binding to the Hg-responsive merR protein has a minimal effect on DNA binding affinity but a significant effect on the localized DNA helical structure (Frantz & O'Halloran, 1990). Likewise, redox chemistry alters the DNA footprint of OxyR rather than markedly affecting the DNA binding affinity (Storz et al., 1990).

ACE1 and AMT1 appear to be the primary sensors of the intracellular Cu^+ concentration in yeast. Basal levels of these proteins must exist in a stable, unactivated state. It is unclear whether the unactivated states of ACE1 and AMT1 are the metal-free molecules or the Zn_4 complexes. The ability of ACE1, and presumably AMT1, to form distinct conformers with Cu^+ and Zn^{2+} may form the basis of the exquisite metal ion specificity in the function of these proteins (Dameron et al., 1993). Metal exchange is facile in ACE1, so Cu^+/Zn^{2+} exchange may be an initial step in Cu-activation if inactive ACE1 or AMT1 states are as ZnACE1 or ZnAMT1.

AMT1 and ACE1 are activated with <5 μM extracellular Cu^{2+} (Thorvaldsen et al., 1993). The all-or-nothing formation of the tetracopper center in AMT1 and presumably ACE1 may be important in making the system responsive to low concentrations of copper. The multiple MT genes in *C. glabrata* and the autoregulation of AMT1 expression enable *C. glabrata* cells to respond to high environmental copper concentrations (Zhou & Thiele, 1993). The efficient coupling

of external copper levels to the concentration of active Cu_4-Zn_1AMT1 allows *C. glabrata* cells to stimulate high-level expression of the three MT genes thereby minimizing Cu-induced toxicity. Thus, the coordination inorganic chemistry involved in Cu^+–thiolate cluster formation in AMT1 appears to be the driving force for copper regulation.

REFERENCES

Allen, M. H., & Hutchens, T. W. (1992) *Rapid Commun. Mass Spectrom. 6*, 308–311.

Andersson, S. G. E., & Kurland, C. G. (1990) *Microbiol. Rev. 54*, 198–210.

Ausubel, F. M., Brent, R., Kingston, R. E., Moore, D. D., Seidman, J. G., Smith, J. E., & Struhl, K. (Eds.) (1993) *Current Protocols in Molecular Biology*, John Wiley & Sons, Inc., New York.

Bertini, I., & Luchinat, C. (1984) *Adv. Inorg. Biochem. 6*, 72–111.

Buchman, C., Skroch, P., Welch, J., Fogel, S., & Karin, M. (1989) *Mol. Cell. Biol. 9*, 4091–4095.

Buchman, C., Skroch, P., Dixon, W., Tullius, T. D., & Karin, M. (1990) *Mol. Cell. Biol.* 10, 4778–4787.

Cramer, S. P., Tehch, O., Yocum, M., & George, G. N. (1988) *Nucl. Instrum. Methods Phys. Res. A266*, 586–591.

Dameron, C. T., Winge, D. R., George, G. N., Sansone, S., Hu, S., & Hamer, D. (1991) *Proc. Natl. Acad. Sci. U.S.A. 88*, 6127–6131.

Dameron, C. T., George, G. N., Arnold, P., Santhanagopalan, V., & Winge, D. R. (1993) *Biochemistry 32*, 7294–7301.

Dance, I., Fisher, K., & Lee, G. (1992) in *Metallothioneins* (Stillman, M. J., Shaw, C. F., III, & Suzuki, K. T., Eds.) pp 284–345, VCH Publishers, Inc., New York.

Dance, I. G. (1979) *J. Am. Chem. Soc. 101*, 6264–6273.

Dance, I. G. (1986) *Polyhedron 5*, 1037–1104.

Dance, I. G., Bowmaker, G. A., Clark, G. R., & Seadon, J. K. (1983) *Polyhedron 2*, 1031–1043.

Fitzgerald, D. W., & Coleman, J. E. (1991) *Biochemistry 30*, 5195–5201.

Frantz, B., & O'Halloran, T. V. (1990) *Biochemistry 29*, 4747–4751

Furst, P., & Hamer, D. (1989) *Proc. Natl. Acad. Sci. U.S.A. 86*, 5267–5271.

Furst, P., Hu, S., Hackett, R., & Hamer, D. (1988) *Cell 55*, 705–717.

Giedroc, D. P., & Coleman, J. E. (1986) *Biochemistry 25*, 4969–4978.

Giedroc, D. P., Qui, H., Khan, R., King, G. C., & Chen, K. (1992) *Biochemistry 31*, 765–774.

Grasetti, D. R., & Murray, J. F., Jr. (1967) *Arch. Biochem. Biophys. 119*, 41–49.

Hamer, D. H. (1986) *Annu. Rev. Biochem. 55*, 913–951.

Hu, S., Furst, P., & Hamer, D. (1990) *New Biologist 2*, 544–555.

Hutchens, T. W., & Allen, M. H. (1992) *Rapid Commun. Mass Spectrom. 6*, 469–473.

Johnson, R. S., & Schachman, H. K. (1983) *J. Biol. Chem. 258*, 3528–3538.

Kosa, J. L., Michelsen, J. W., Louis, H. A., Olsen, J. I., Davis, D. R., Beckerle, M. C., & Winge, D. R. (1994) *Biochemistry 33*, 468–477.

Lane, R. W., Ibers, J. A., Frankel, R. B., Papaefthymiou, G. C., & Holm, R. H. (1977) *J. Am. Chem. Soc. 99*, 84–97.

Lytle, F. E. (1970) *Appl. Spectrosc. 24*, 319–326.

Maret, W., Andersson, I., Dietrich, H., Schneider-Bernlohr, H., Einarson, R., & Zeppezauer, M. (1979) *Eur. J. Biochem. 98*, 501–512.

Mastropaolo, D., Thich, J. A., Potenza, J. A., & Schugar, H. J. (1977) *J. Am. Chem. Soc. 99*, 424–428.

Michael, S. F., Kilfoil, V. J., Schmidt, M. H., Amann, B. T., & Berg, J. M. (1992) *Proc. Natl. Acad. Sci. U.S.A. 89*, 4796–4800.

Michelsen, J. W., Sewell, A. K., Louis, H. A., Olsen, J. I., Davis, D. R., Winge, D. R., & Beckerle, M. C. (1994) *J. Biol. Chem. 269*, 11108–11113.

Nakagawa, K. H., Inouye, C., Hedman, B., Karin, M., Tullius, T. D., & Hodgson, K. O. (1991) *J. Am. Chem. Soc. 113*, 3621–3623.

Nicholson, J. R., Abrahams, I. L., Clegg, W., & Garner, C. D. (1985) *Inorg. Chem. 24*, 1092–1096.

Nye, J. A., Petersen, J. M., Gunther, C. V., Jonsen, M. D., & Graves, B. J. (1992) *Genes Dev. 6*, 975–990.

Pickering, I. J., George, G. N., Dameron, C. T., Kurz, B., Winge, D. R., & Dance, I. E. (1993) *J. Am. Chem. Soc. 115*, 9498–9505.

Storz, G., Tartaglia, L. A., & Ames, B. N. (1990) *Science 248*, 189–194.

Swenson, D., Baenziger, N. C., & Coucouvanis, D. (1978) *J. Am. Chem. Soc. 100*, 1932–1934.

Szczypka, M. S., & Thiele, D. J. (1989) *Mol. Cell. Biochem. 9*, 421–429.

Thiele, D. J. (1988) *Mol. Cell. Biol. 8*, 2745–2752.

Thiele, D. J. (1992) *Nucleic Acids Res. 20*, 1183–1191.

Thorvaldsen, J. L., Sewell, A. K., McCowen, C. L., & Winge, D. R. (1993) *J. Biol. Chem. 268*, 12512–12518.

Welch, J., Fogel, S., Buchman, C., & Karin, M. (1989) *EMBO J. 8*, 255–260.

Xu, B., Krudy, G. A., & Rosevear, P. R. (1993) *J. Biol. Chem. 268*, 16259–16264.

Yu, X., Wojciechowski, M., & Fenselau, C. (1993) *Anal. Chem. 65*, 1355–1359.

Zhou, P., & Thiele, D. J. (1991) *Proc. Natl. Acad. Sci. U.S.A. 88*, 6112–6116.

Zhou, P., & Thiele, D. J. (1993) *Genes Dev. 7*, 1824–1835.

Zhou, P., Szczypka, M. S., Sosinowski, T., & Thiele, D. J. (1992) *Mol. Cell. Biol. 12*, 3766–3775.